Chapter 9
Predicting Permeability in the Target Reservoirs on the Rock Springs Uplift, Southwest Wyoming

Yuri Ganshin

Abstract Estimates of permeability in carbonate rocks from porosity alone are highly uncertain but can be improved when pore geometry information is incorporated. We developed a permeability model for a 400-ft-thick carbonate reservoir on the Rock Springs Uplift, Wyoming, with the objective of increasing the accuracy of flow simulation during CO_2 sequestration. Core data was used to identify hydraulic flow units within the reservoir and to further distinguish them through lithofacies analysis of thin sections. We used both the *Flow Zone Indicator* (FZI) and *Winland's* R_{35} method to identify the flow units. FZI and pore throat radius values were obtained from the log-of-permeability-versus-porosity crossplot of the core sample measurements. For the rock types composing the Madison Limestone on the Rock Springs Uplift, both the FZI and R_{35} methods proved to be effective techniques for rock-type classification. We found that acoustically derived porosity estimates within the Madison Limestone stratigraphic interval correlate well with those derived from the FZI. Sonic velocity in carbonates is a function not only of total porosity but also of the predominant pore type that determines the permeability of the rock. Hence our permeability estimation used both the density porosity and calibrated sonic porosity from conventional wireline logs. In the Madison Limestone, vug development within dolomitized sparitic carbonates has resulted in layered structures of super-permeable zones sandwiched between non-vuggy, less permeable micritic dolostones. Among the various vuggy zones of the Madison stratigraphic interval, permeability was found to vary by two to three orders of magnitude.

We also estimated the permeability in a 670-ft-thick sandstone unit within the Weber Sandstone on the Rock Springs Uplift with the objective of increasing the accuracy of our CO_2 flow simulation program. We used core data to identify the porosity-permeability relationship for the cored depth interval. On the basis of this relationship and well log data, we constructed a continuous vertical permeability profile. Seismically derived porosity values along the Weber horizon were used to model spatial permeability variations away from the RSU #1 well. The resulting

Y. Ganshin (✉)
Carbon Management Institute Laramie, University of Wyoming, Laramie, USA
e-mail: yganshin@uwyo.edu

R. C. Surdam (ed.), *Geological CO_2 Storage Characterization,*
Springer Environmental Science and Engineering, DOI 10.1007/978-1-4614-5788-6_9,

statistical estimators of the permeability distribution led us to classify the Weber Sandstone as highly heterogeneous and variably permeable strata.

9.1 The Madison Limestone Reservoir

9.1.1 Methodology

Reliable knowledge of permeability can only be derived from laboratory analysis of core samples. However, that procedure becomes impractical for thick reservoir sections or poorly cored wells. Instead, permeability is commonly estimated in uncored sections or poorly cored wells from the following permeability-versus-porosity relationship—which has no apparent theoretical basis.

$$\log(k) = a\varphi + b \tag{9.1}$$

In Eq. 9.1, permeability (k) is plotted as a log function merely because it is assumed to be log-normally distributed with respect to porosity (φ).

Estimates of permeability derived from porosity alone are very ineffective. The uncertainty arises because porosity is a volumetric parameter: it is the ratio of pore volume to bulk volume. Permeability, on the other hand, is a measure of the flow properties of a fluid through the pores, which depends not only on the volumetric proportion of the pore space but also on its geometric distribution and connectivity. Combining these non-volumetric parameters with porosity significantly improves estimates of permeability. Further significant improvement can be obtained by grouping core data on the porosity/permeability plots by rock type.

Rock typing can be understood as a process of classifying reservoir rocks into distinct units, each of which was deposited under similar geologic conditions and has undergone similar diagenetic alteration. When properly classified, a given rock type is characterized by a unique mineralogy (type, abundance, morphology), texture (grain size, grain shape, sorting, packing), pore geometry, and porosity/permeability relationship. Hence, rock typing narrows the search domain of realistic permeability solutions in uncored intervals and in uncored wells.

Of the various quantitative rock-typing techniques presented in the literature (Gunter et al. 1997; Hartmann and Farina 2004; Amaefule et al. 1993; Porras and Campos 2001; Jennings and Lucia 2001; Guo et al. 2007), two techniques—the FZI (Amaefule et al. 1993) and Winland's R_{35} (Gunter et al. 1997)—appear to be more widely used than the others for siliciclastic and carbonate reservoirs.

The FZI Technique Amaefule et al. (1993) found that core data provides information on various depositional and diagenetic controls on pore geometry, and that variations in pore geometry attributes lead to the definition of separated zones (hydraulic flow units) with similar flow properties. They proposed a method based

mainly on the Kozeny-Carmen equation (Carmen, 1937) and the concept of the mean hydraulic unit radius (Bird et al. 1960).

The verification of hydraulic-unit zonation on the log-of-permeability-versus-porosity crossplot is necessarily the first step in their proposed method. Next, the Flow Zone Indicator (FZI) is computed for each data point on the crossplot:

$$FZI[\mu] = RQI / \varphi_Z \tag{9.2}$$

using the Reservoir Quality Index (RQI),

$$RQI[\mu] = 0.0314\sqrt{(k / \varphi)}$$

where μ indicates that FZI and RQI are computed in micrometers, k is permeability measured in millidarcy [mD] and φ is porosity [decimal fraction]—and the pore-volume-to-grain-volume ratio (φ_Z),

$$\varphi_Z = \varphi/(1-\varphi)$$

Then, Eq. 9.2 is rearranged for the estimation of permeability k from porosity φ and FZI (i.e., rock type):

$$k(mD) = 1014\varphi^3 (FZI / (1-\varphi))^2 \tag{9.3}$$

Winland's R_{35} Technique Winland developed an empirical relationship among porosity, air permeability, and the pore aperture corresponding to a mercury non-wetting phase of 35 % (R_{35}) for a mixed suite of sandstones and carbonates. Through multiple regression analysis, Winland came up with an equation published by Kolodzie (1980),

$$\log(R_{35}) = 0.732 + 0.588\log(k_a) - 0.864\log(\varphi) \tag{9.4}$$

where R_{35} is the pore aperture radius (μ, micrometers), k_a is the uncorrected air permeability (mD), and φ is porosity (decimal fraction).

Core samples of a given rock type have similar R_{35} values that can be used to define major flow units in reservoirs (Gunter et al. 1997). Similarly to the FZI method, the R_{35} radius (and corresponding rock type) can be estimated on the crossplot of the log of permeability versus porosity built from the cores. Data from laboratory measurements can be further used to develop the hydraulic unit (rock type) tracks and regression models from wireline logs. Permeability for uncored well intervals can then be predicted using the same Winland's R_{35} equation (Eq. 9.4). Both techniques (FZI and R_{35}) have been applied successfully to both clastic-type and carbonate-type reservoirs (Amaefule et al. 1993; Gunter et al. 1997).

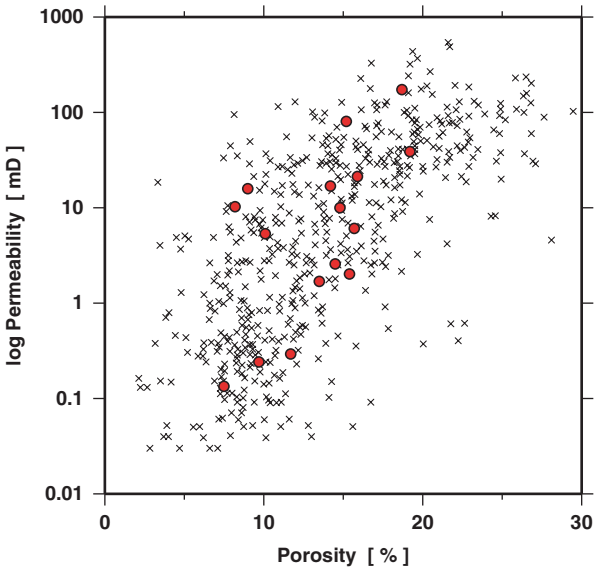

Fig. 9.1 Simple semilog plot of permeability vs. porosity for dolostones of the Madison Formation. Crosses mainly represent outcrop samples from Ehrenberg et al. (2006). Red dots—core samples from the RSU #1 well, Rock Springs Uplift, Wyoming. Pearson's correlation coefficient for the RSU dataset $\mathbf{R} = 0.50$, coefficient of determination $\mathbf{R^2} = 0.25$

9.1.2 Permeability Modeling

The porosity-permeability relationship varies considerably in different facies of the Madison Limestone. It is more difficult to predict permeability in carbonate rocks than in sandstones because carbonate pore geometry can be very complex. Fig. 9.1 shows a typical porosity-permeability relationship for dolostones of the Madison Limestone with a coefficient of determination $\boldsymbol{R^2}$ of 0.24. Even for core samples taken throughout the RSU #1 well, the spread of permeability measurements reaches three orders of magnitude (red dots in Fig. 9.1) with low correlation ($\boldsymbol{R^2} = 0.25$). It is immediately apparent from Fig. 9.1 that there is no clear correlation between porosity and permeability, which makes it difficult to predict permeability even in cases with a redundant amount of core and laboratory measurements. Therefore, a practical method or workflow to partition the pore types and distinguish rock facies by means of wireline logs is essential for permeability estimation.

In this study, we first test the concept of grouping porosity and permeability data according to their FZI/R_{35} values. Next, we note that different log responses correlate differently with these numbers, and we find that acoustically measured porosity shows the strongest correlation. Finally, using this correlation, we construct a permeability profile for the whole Madison stratigraphic interval.

The laboratory data used in this study are from RSU #1 core plug samples measured at Intertek Westport Technology Center, Houston, Texas. The data include porosity and Klinkenberg-corrected permeability values obtained at reservoir conditions. Fig. 9.2 shows a plot of the porosity/permeability variations in this dataset. The dots represent measured data (red dots in Fig. 9.1); the curves indicate porosity/permeability models calculated from Eq. 9.3 (Fig. 9.2a) and from Eq. 9.4

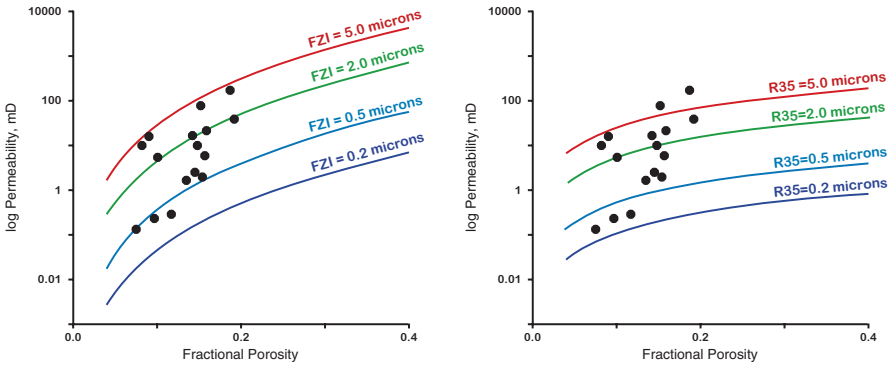

Fig. 9.2 Semilog plot of permeability vs. porosity for the Middle Madison dolostone, RSU #1 well, Rock Springs Uplift, Wyoming. Dots are core samples from the RSU #1 well (red dots in Fig. 9.1). The colored curves indicate constant hydraulic units (rock types) defined through the *FZI* value (*left*) and the R_{35} value in microns (*right*)

(Fig. 9.2b). The corresponding FZI and R_{35} values used for modeling are labeled over the curves in Fig. 9.2. For both types of models, porosity and permeability correlate very well along an interval with constant FZI or R_{35} value. At the same porosity, samples with higher FZI or R_{35} values have higher permeability. Thus, the FZI and R_{35} values can be understood to denote pore connectivity (hydraulic zones); given the same volumetric pore space, higher connectivity would produce greater permeability along with higher FZI and R_{35}. Both the FZI and R_{35} curves tend to ascend with increasing porosity, and both modeled parameters have approximately the same range (0.2–5.0 μ) corresponding to the set of measured porosity/permeability values (Fig. 9.2). The correlation coefficient between the FZI and R_{35} models for the Madison set of measurements is 0.860. Despite on the overall similarity, there is a systematic difference between the two models: the FZI curves are steeper than the R_{35} curves.

Selecting the wireline data for the derivation of the transform equation was the next step in our modeling study. The following wireline logs were used for statistical analysis: gamma ray (GR), photo electric section (PE), density (DEN), P-wave velocity (VEL), neutron porosity (NPHI), focused conductivity—DOI 60 inch (COND), resistivity—DOI 60 inch (RES), density porosity (DPHI), and vuggy porosity (VPHI). The vuggy porosity log was calculated as the difference between density porosity and sonic porosity. The log values were extracted at exactly the same depths as the core plugs. Table 9.1 shows a matrix of the logs together with the calculated FZI and R_{35} values at all the core depths of the Madison Limestone stratigraphic interval. A statistical evaluation of the correlation strength between wireline data and modeled attributes (FZI and R_{35} values) was performed for each log. The cross correlation coefficients for the FZI and R_{35} prediction models are shown at the bottom of each column in Table 9.1.

Positive correlation coefficients designate direct correlation, in which large values of one variable are associated with large values of the other, and small with

Table 9.1 Modeling and log data for regression analysis

Depth	FZI	R35	GR	PE	DEN	VEL	NPHI	COND	RES	DPHI	VPHI
12344.0	3.921	3.432	8.98	2.830	2.555	17979	20.23	299.4	3.340	16.84	6.72
12349.5	1.772	4.060	10.89	3.028	2.419	15327	28.02	1163.8	0.859	24.12	7.79
12352.0	4.220	4.111	12.53	2.922	2.356	15221	32.78	1214.9	0.823	27.49	11.47
12354.0	4.021	6.764	14.47	3.186	2.400	16449	30.09	945.0	1.058	25.13	12.30
12356.0	1.879	3.610	15.64	3.174	2.493	17592	24.49	675.8	1.480	20.16	9.69
12357.5	1.561	2.693	20.18	2.906	2.544	17939	22.83	584.3	1.711	17.43	8.16
12362.5	0.623	0.766	16.15	3.230	2.522	17485	23.10	704.7	1.419	18.61	7.95
12366.5	1.102	2.196	15.37	2.969	2.429	15674	29.54	1141.3	0.876	23.58	9.10
12371.0	1.191	2.112	12.40	3.082	2.473	16661	24.62	844.0	1.185	21.23	8.20
12373.0	2.064	2.864	11.74	3.195	2.516	17256	22.40	526.2	1.900	18.93	7.30
12375.0	1.361	1.933	13.23	2.957	2.590	18379	17.55	292.9	3.412	14.97	5.26
12382.0	1.122	1.095	13.09	3.162	2.624	18978	16.22	229.7	4.353	13.16	4.80
12383.5	0.461	0.328	19.86	3.554	2.633	18682	15.46	231.7	4.316	12.67	3.60
12385.0	0.918	0.897	14.80	3.242	2.594	18042	17.93	244.6	4.088	14.76	4.63
12394.0	0.930	1.147	11.24	3.189	2.577	17359	19.31	288.3	3.468	15.67	4.29
12399.5	0.374	0.312	11.72	2.960	2.534	17100	21.46	353.5	2.829	17.97	5.97
12400.5	0.794	0.847	13.04	3.174	2.519	16922	22.38	347.7	2.876	18.77	6.42
12404.0	1.342	1.568	11.63	2.864	2.483	16552	25.86	312.5	3.200	20.70	8.16
12406.5	0.782	0.937	11.21	2.827	2.503	16741	23.90	283.7	3.524	19.63	7.15
12407.0	1.418	2.404	10.93	2.727	2.515	16866	24.15	279.7	3.574	18.98	7.20
12408.0	0.533	0.569	12.91	2.612	2.544	16957	24.77	276.2	3.620	17.43	6.82
12410.0	2.192	3.264	14.06	2.835	2.486	17001	25.15	261.7	3.822	20.53	8.85
12414.0	1.415	2.322	11.86	3.537	2.603	17940	17.56	141.7	7.056	14.28	3.97
12414.5	1.481	2.029	13.30	3.555	2.640	18116	16.23	138.3	7.213	12.30	2.64
12415.0	1.048	1.442	14.73	3.548	2.671	18173	16.27	140.0	7.123	10.64	1.91
12421.0	4.152	8.894	17.20	3.002	2.455	17250	24.40	232.5	4.301	22.19	10.06
12422.0	2.766	5.902	16.82	2.877	2.505	17538	22.90	215.7	4.635	19.52	8.49
12429.0	1.213	2.144	15.45	2.894	2.627	18517	18.41	74.5	13.424	12.99	4.87
12432.5	0.543	0.352	10.88	4.497	2.767	19757	12.73	33.3	29.926	5.51	0.56
12434.5	0.870	1.423	27.61	3.193	2.688	19548	15.47	40.1	24.901	9.73	3.69
12437.5	1.513	1.052	14.19	2.986	2.614	18443	18.45	65.6	15.245	13.69	5.12
12447.0	0.710	0.754	9.96	2.789	2.695	19820	14.88	42.5	23.536	9.36	3.68
12448.0	0.679	0.705	8.87	2.952	2.724	19555	13.75	41.4	24.139	7.81	1.86
12454.0	0.800	0.998	13.78	3.392	2.651	18889	18.79	44.6	22.418	11.71	5.10
12459.0	0.710	0.772	8.70	2.930	2.768	21510	12.35	43.3	23.059	5.45	3.16
12461.5	3.263	4.571	15.68	3.196	2.580	18920	23.28	102.8	9.724	15.51	9.27
12462.5	3.522	5.452	17.73	3.247	2.550	18027	24.89	137.5	7.273	17.11	9.08
12466.5	3.609	3.576	19.87	3.101	2.561	17627	23.24	163.8	6.107	16.52	7.16
12476.5	3.664	7.773	7.77	3.140	2.541	17749	24.17	84.1	11.890	17.59	8.44
12478.5	2.032	1.959	7.74	3.075	2.604	17790	20.48	67.2	14.890	14.22	5.00
12492.0	0.526	0.421	10.35	4.094	2.744	19740	12.99	5.2	190.95	6.74	1.27
12505.0	2.725	1.351	14.42	2.599	2.625	18748	17.23	179.3	5.578	13.10	4.82
12512.5	1.927	2.994	13.68	4.090	2.770	22725	9.05	42.4	23.497	5.35	3.09
12513.0	2.428	5.032	13.71	4.060	2.774	23370	9.02	30.5	32.655	5.13	3.80
12514.0	2.068	2.373	11.15	4.645	2.778	23777	8.97	15.3	65.327	4.92	4.17
R_{FZI} =	1.00	0.860	0.078	−.115	−.393	−.139	0.401	0.183	−.194	0.393	0.612
R_{R35} =	0.860	1.00	0.122	−.057	−.411	−.138	0.403	0.195	−.187	0.411	0.633

small. Negative coefficients indicate the opposite. Analysis of the data shown in Table 9.1 demonstrates that the strongest positive correlation exists between the modeled attributes and the vuggy porosity. In both cases, the correlation coefficient ***R*** is greater than 0.6, which means that vuggy porosity is an attribute that directly correlates with the pore connectivity and can be used to estimate permeability. After substituting the vuggy porosity and corresponding regression coefficients for the unavailable variable FZI in Eq. 9.3, we obtain—after some algebraic rearrangement—the following formula to estimate permeability in the Madison Limestone:

$$k = 63\varphi^3\left(VPHI/\left(1-\varphi\right)\right)^2, \tag{9.5}$$

where *VPHI* is vuggy porosity (computed as the difference between density porosity and sonic porosity). We used fractional density porosity values as parameter φ. By use of Eq. 9.5, a synthetic permeability log was generated for the whole Madison stratigraphic interval (Fig. 9.3). Using a similar approach for the R_{35} attribute and Eq. 9.4, we also modeled permeability for the same interval:

$$\log(k) = 1.7\left[\log\left(0.502\ VPHI - 1.089\right) + 0.864\ \log\left(\phi\right) - 0.732\right]$$

Both specific formulas that we used for permeability modeling are of local applicability only; however, the described methodology is of general applicability, and can be used at different locations and with different rock types.

We used laboratory measurements on the Madison cores to test the validity of our multivariate permeability models (Eqs. 9.4 and 9.5) and to compare them with a univariate linear regression model based on Eq. 9.1. The measured data and permeability estimates for the three models are shown in Table 9.2. A better match between calculated and measured data is demonstrated by the higher correlation coefficients where the models with two independent variables (total porosity and vuggy porosity) were used for permeability estimation than where the conventional, univariate porosity-permeability model was used. This means that porosity and permeability correlate well within an established hydraulic unit or, in other words, for a given pore type. At the same total porosity, carbonate rocks with higher values of vuggy porosity have higher permeability. In this study, both bivariate models demonstrate equally moderate correlation with the laboratory measurements. We believe that the slightly higher correlation coefficient for the R_{35} model than that for the FZI model (Eq. 9.4 vs. Eq. 9.5) is not statistically significant.

Permeability Distribution A histogram and cumulative histogram of the permeability distribution and associated statistical estimators of average permeability for the middle Madison reservoir are shown as Fig. 9.11 in Sect. 9.2.2. Following a description of the various average estimators for a statistical distribution as applied to the Weber Sandstone, a discussion in Sect. 9.2.2.2 compares the estimated average permeability of the middle Madison with that of the Weber Sandstone.

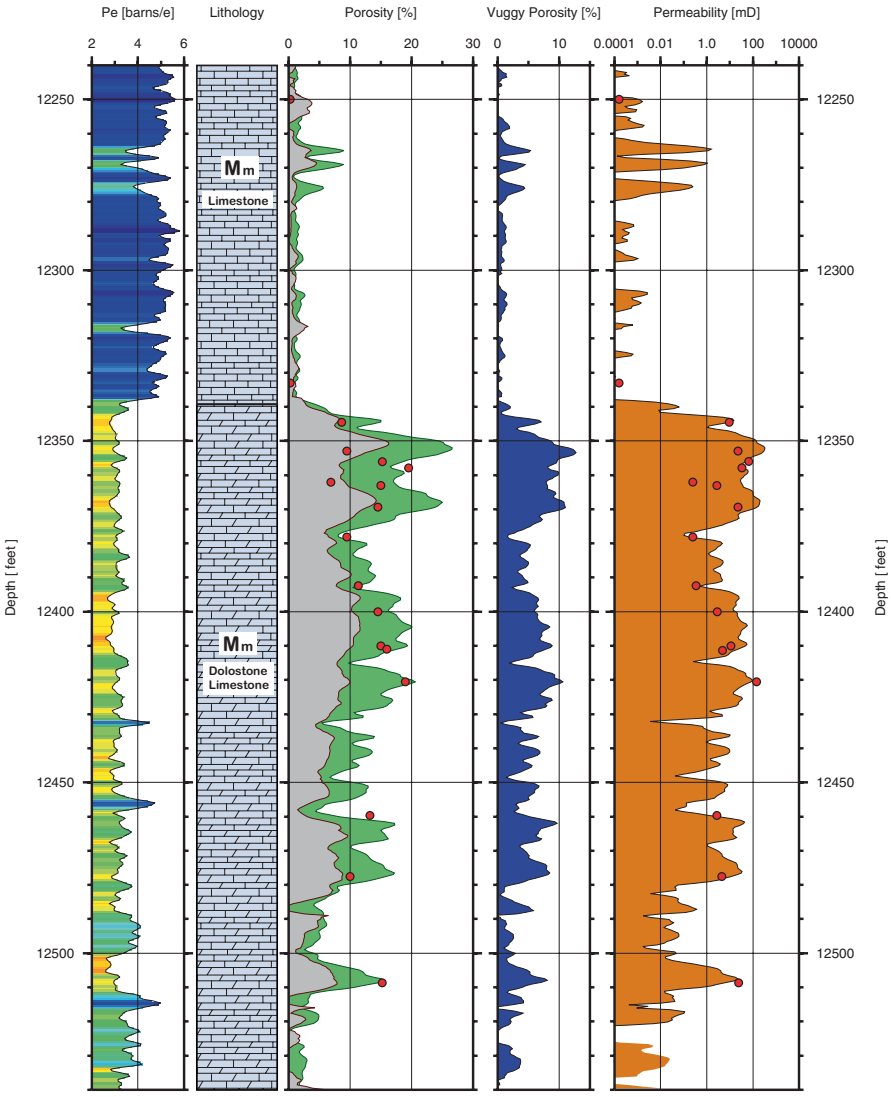

Fig. 9.3 Open-hole logs and core data in the Madison Formation in the RSU #1 well. Tracks from left to right are (1) photo electric section, (2) lithology, (3) density (*green*) and sonic (*gray*) porosity with total porosities from core (*red dots*), (4) sonic-vug porosity index (difference between density and sonic porosities), (5) permeability from logs (*orange*) overlaid with core measurements (*red dots*)

9.1.3 Discussion

To understand the good correlation between vuggy porosity and permeability reported in Table 9.1 for the Madison cores, we first examine the FZI attribute.

Table 9.2 Measurements and Modeling Results

Lab-measured porosity, %	Log-measured vug porosity, VPHI, %	Lab-measured permeability, mD	Modeled (Eq. 1) permeability, mD	Modeled (Eq. 5) permeability, mD	Modeled (Eq. 4) permeability, mD
8.20	6.72	10.20	1.25	1.86	5.11
22.40	7.79	59.44	68.69	71.39	32.01
9.00	11.47	15.90	1.57	7.30	19.74
15.20	12.30	80.10	9.02	46.55	49.28
19.20	9.69	38.80	27.87	64.14	41.86
18.00	8.16	21.44	19.87	36.37	25.85
15.40	7.95	2.01	9.57	20.32	19.35
21.40	9.10	19.55	51.81	82.70	42.69
19.20	8.20	15.59	27.86	45.88	28.72
14.20	7.30	16.80	6.80	13.06	14.03
15.50	5.26	9.80	9.82	9.08	6.73
11.30	4.80	2.34	3.00	2.67	3.23
9.70	3.60	0.24	1.91	0.91	0.92
11.70	4.63	1.76	3.36	2.77	3.02
14.50	4.29	3.65	7.41	4.83	3.22
11.70	5.97	0.29	3.36	4.61	6.33
13.00	6.42	1.86	4.85	7.53	8.94
13.00	8.16	5.30	4.85	12.17	16.03
14.50	7.15	2.59	7.41	13.43	13.76
18.00	7.20	17.68	19.87	28.33	19.22
13.90	6.82	1.04	6.25	10.61	11.49
15.00	8.85	22.75	8.53	23.04	23.81
17.50	3.97	15.99	17.25	7.82	3.22
14.80	2.64	9.94	8.06	1.96	0.26
15.70	1.91	6.06	10.39	1.25	0.06
18.70	10.06	173.00	24.20	63.08	43.69
19.80	8.49	93.67	33.00	54.84	32.61
19.10	4.87	15.88	27.09	15.93	7.30
8.60	0.56	0.23	1.40	0.02	0.03
18.80	3.69	7.73	24.89	8.63	2.67
7.70	5.12	1.24	1.09	0.88	2.23
13.20	3.68	1.56	5.13	2.61	1.58
13.00	1.86	1.36	4.85	0.63	0.05
15.00	5.10	3.03	8.53	7.65	5.87
13.50	3.16	1.68	5.59	2.06	0.79
13.30	9.27	33.81	5.28	16.95	22.15
14.40	9.08	51.26	7.20	21.18	23.77
9.40	7.17	13.37	1.76	3.27	7.31
18.90	8.44	139.74	25.61	46.08	30.03
10.10	5.00	5.34	2.14	2.01	3.10
10.60	1.27	0.42	2.47	0.15	0.04
4.90	4.82	0.98	0.49	0.19	0.96
15.90	3.09	21.40	10.99	3.42	0.89
19.70	3.80	70.88	32.08	10.79	3.24
11.90	4.17	9.42	3.56	2.38	2.18
Correlation	*Coefficient*	*R = 1.0*	*R = 0.473*	*R = 0.649*	*R = 0.664*

According to Amaefule et al. (1993), the FZI is inversely related to a product of pore parameters (shape factor, tortuosity, and surface-area-to-grain-volume ratio) and reflects connectivity between pores (greater FZI implies greater connectivity). This is a unique and useful attribute that allows us to quantify the flow character of a reservoir and lets us average the rock properties at a small scale, such as core plugs, and compare them with larger-scale variations at, for example, well-bore scale. We consider that FZI and R_{35} are the most reliable quantitative attributes for geometrical pore structure characterization in carbonates, and that these attributes can be directly related to sonic and density readings on wireline logs.

A characteristic of carbonate reservoirs is significant variability in petrophysical properties, especially permeability, because carbonates are subject to rapid and pervasive diagenetic alteration. Such alteration, particularly cementation and dissolution processes, continuously modifies the pore structure to create or destroy porosity, and in extreme cases can mean a complete change in mineralogy from calcite to dolomite. All such modifications alter the elastic properties of the rock, particularly density and sonic velocity. The result is a wide range of density and velocity within carbonates, as observed in the Madison stratigraphic interval where compressional-wave velocity ranges from 15,000 to 24,000 ft/s (4,600–7,300 m/s), and density from 2.35 to 2.85 g/cc (Fig. 9.4).

Porosity is the main controlling factor in determining sonic velocity in rocks; this fact established acoustic logging as an essential borehole measurement. However, in carbonates the pore type is nearly as important in elastic behavior and the resultant sonic velocity. For example, at equal total porosities, moldic or intrafossil pore types allow significantly higher velocities than those allowed by pore types that are embedded in a rigid rock framework, such as interparticle porosity or microporosity (Anselmetti and Eberly 1999).

Sonic and density logs are common measurements in carbonate drill holes. Converting the sonic log to sonic porosity by applying the Wyllie time-average equation (Wyllie et al. 1956) is a widely used method for producing sonic porosity (Schlumberger 1974; Rider and Kennedy 2011). In holes where both tools are run, comparing the two porosity values yields a difference that is commonly termed *secondary porosity* and is quantified with the secondary porosity index, SPI (Schlumberger 1974). The SPI reflects to the presence of vugs and fractures (Schlumberger 1974; Lucia 1999; Doveton 1994) that are not detected by the sonic signal but are detected by the density and neutron-porosity logs.

Mavko and Mukerji (1995), among others, provided the theoretical explanation of this acoustic velocity behavior. High-aspect-ratio pores, such as molds and vugs, provide more grain-to-grain contact than do interparticle and intercrystalline pores. Thus, at equal total porosity, moldic and vuggy types of porosity decrease the pore compressibility and provide more stiffness to the rock, making acoustic velocity higher than in a formation with predominantly intercrystalline porosity.

Many scientists have attempted to estimate quantitatively the influence of vuggy porosity on acoustic logs. Some of them proposed empirical equations, while others just documented a broad range of scatter in velocities at a given porosity. Following Xu et al. (2006) we use the terms “vug” and “vuggy” to refer to voids that are either visually identifiable in thin section images or recognizable through specific

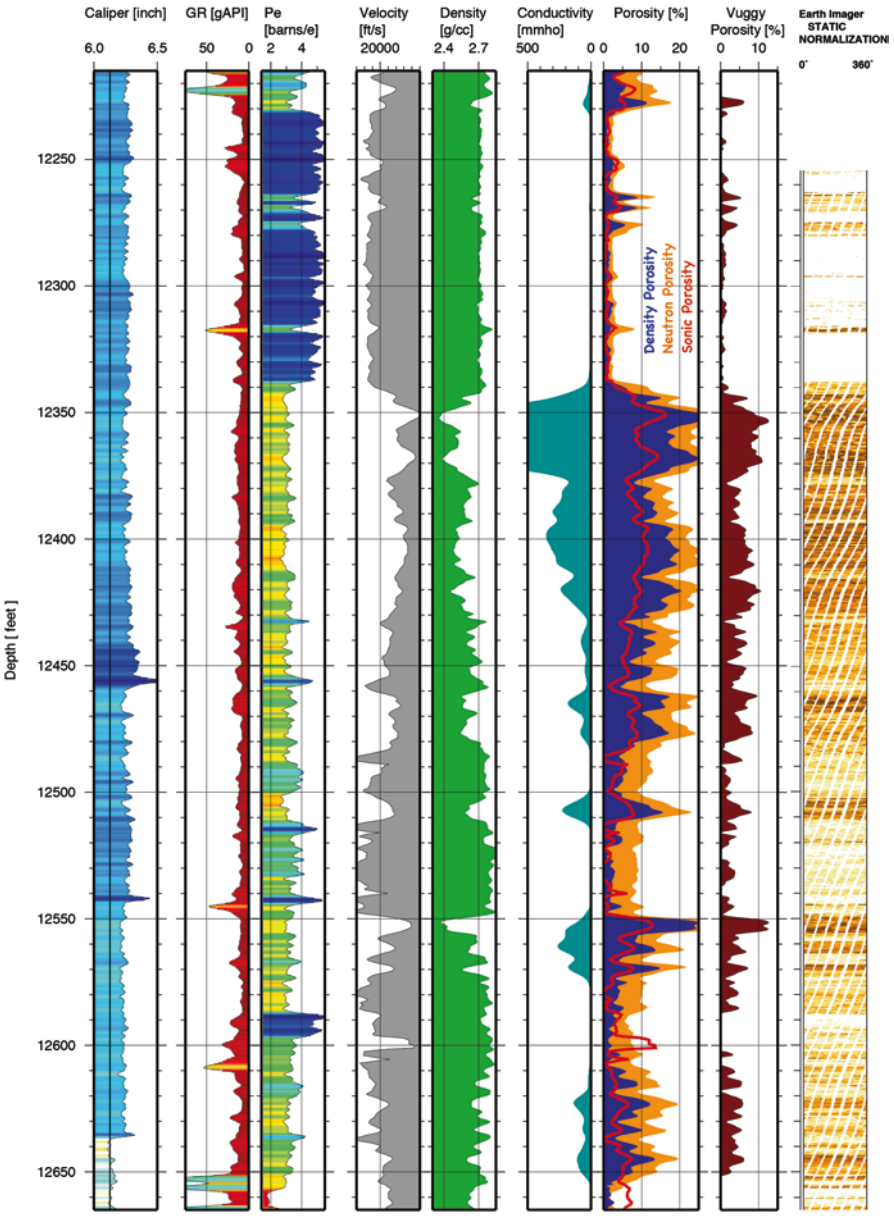

Fig. 9.4 Open-hole wireline logs from the RSU #1 well for the Madison stratigraphic interval. Porosity panel shows neutron porosity log (*orange bar-graph*) overlaid with the neutron-density crossplot porosity (*blue bar-graph*). The red plot in the Porosity panel represents calculated sonic-log porosity. The Vuggy Porosity panel represents the difference between density and sonic porosity. The rightmost panel shows the Baker Hughes micro-resistivity image log with darker colors representing more conductive rock textures

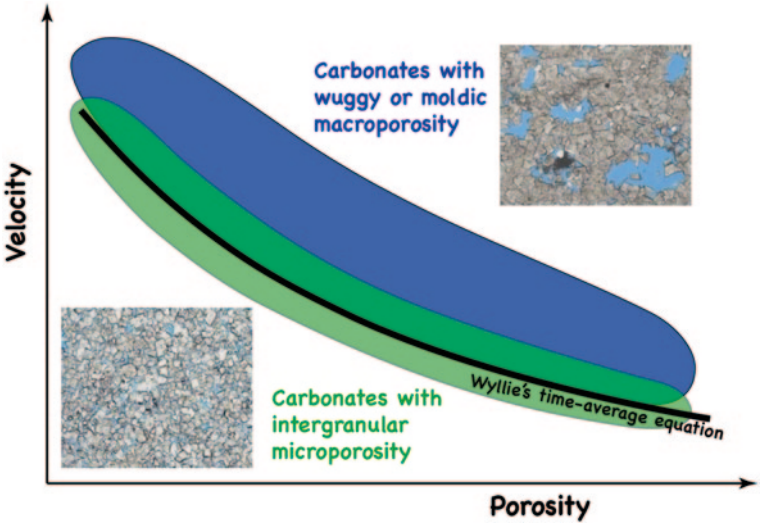

Fig. 9.5 Cartoon showing the velocity-porosity relationship in carbonate rocks. A first-order inverse relation between velocity and porosity follows the Wyllie's time-average equation regardless of the pore structure. Differences in the pore structure produce a second-order variation on velocity at a given porosity: samples with vuggy or moldic porosity tend to fall into the high-velocity area, whereas samples dominated by microporosity tend to cluster around the time-average trend line. The corresponding thin-section images illustrating the difference in the pore structure are actual Madison Formation samples from the RSU #1 well

well-log signatures such as micro-resistivity images (rightmost panel in Fig. 9.4). In this study we use *primary porosity* to refer to the microporosity homogeneously represented in the cores, and *secondary porosity* to refer to the heterogeneously distributed porosity, which commonly correlates with vuggy or moldic porosity.

Weger et al. (2009) analyzed the velocity-porosity relationship of water-saturated carbonate samples and noticed that samples with vuggy or moldic porosity tend to fall into the high-velocity area, while samples with great amounts of microporosity tend to cluster around the Wyllie time-average equation in the lower part of the velocity-porosity data cloud (Fig. 9.5). Although most samples contain more than one pore type, at any given porosity a trend of increasing velocity with decreasing microporosity is observed (Weger et al. 2009). This observation allows us to conclude that vugs, especially spherical vugs in carbonates, have little effect on compressional sonic waves and cause the sonic (Wyllie's) porosity to read too low. Therefore, the difference between the density and sonic porosities can be regarded as a measure of vuggy porosity.

Data from the Madison Limestone on the Rock Springs Uplift support this statement. For example, the difference between the total porosity (derived from the density log) and the sonic porosity—referred to here as vuggy porosity—correlates well with the secondary or vuggy porosity visible on the micro-resistivity image log from the RSU #1 well (Fig. 9.4). The methodology described in this study uses

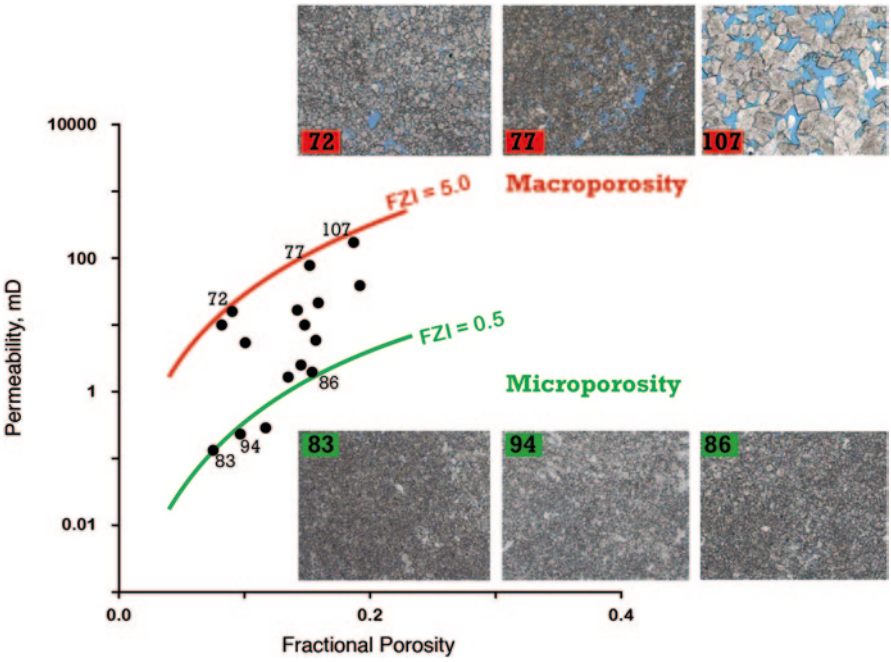

Fig. 9.6 Semilog plot of permeability vs. porosity for the Madison Limestone samples, RSU #1 well, Rock Springs Uplift, Wyoming. The colored curves indicate constant hydraulic units defined by the *FZI* value. Thin section images (labeled with the sample ID numbers) demonstrate that permeability of the corresponding dolostone sample is a function of the total porosity and the pore structure. Dolostones dominated by large vuggy pore types (*top*) show greater permeability than fine-grained dolostones dominated by intergranular microporosity (*bottom*)

attributes (FZI and R_{35}) that quantify the relationship between porosity, permeability, and pore geometry. Carbonate rocks characterized by secondary porosity (large vuggy and moldic pores) in addition to the primary porosity within the matrix have both macroporosity and microporosity. In our methodology, macropores are defined by pores that display the bright colors of the blue epoxy filling the pores in thin section. Samples with great amounts of intergranular microporosity cluster along the low-value FZI curves; they are related to low-permeability dolostones facies in our dataset (Fig. 9.6). In contrast, samples containing moldic and vuggy porosity reveal the highest measured permeability and corresponding FZI values.

The fairly strong correlation between FZI/R_{35} attributes and macroporosity illustrates the importance of considering geometrical pore typing for permeability modeling. Following Amaefule et al. (1993), we define a hydraulic unit as a geologic zone that has a distinct expression in the FZI domain and that controls the permeability of a formation.

9.1.4 Conclusion

Modeling permeability in heterogeneous carbonate reservoirs can be challenging due to significant spatial variations in pore geometry. In this study, we have shown that the log-derived vuggy porosity in carbonates correlates well with the Flow Zone Index and Winland's R_{35} radius, methods often used to define major flow units in reservoirs. We used both methods to model facies and permeability across the whole Madison Limestone stratigraphic interval (~ 400 ft thick) using relatively sparse data from laboratory measurements and wireline logs. A fairly high correlation coefficient observed in the estimated-versus-measured core permeability was achieved—an important objective of this study. Our results indicate that capturing complex variations in pore geometry within a rock is the key to successful permeability modeling. We have demonstrated that vuggy and moldic macroporosity must not be ignored in modeling, and that a carbonate interval should be approached as a dual-porosity system. The challenge in predicting permeability is constructing a model that effectively incorporates both types of porosity—homogeneous microporosity and heterogeneous vuggy porosity—without becoming too complex. We have shown that the subdivision of a carbonate reservoir into hydraulic units based on the vuggy porosity index can be routinely performed in most situations, and that this greatly enhances permeability prediction in heterogeneous reservoirs.

9.2 The Weber Sandstone Reservoir

9.2.1 Permeablity Estimation

The most obvious control on permeability is porosity. However, permeability also depends upon the interconnectivity of the pores, and that in turn depends on the size and shape of grains, the grain size distribution, and such other factors as wetting properties of the rock and diagenetic history. For the Weber Sandstone reservoir, some generalizations can be made:

- The smaller the grains, the smaller the pores and pore throats, and the lower the permeability.
- Secondary porosity is negligible; thus, the bulk permeability is controlled solely by matrix (primary) porosity.

Under these assumptions and based on empirical knowledge (e.g., Archie 1950; Nelson 1994; Nelson 2004), permeability can be estimated from the relationship

$$\log(k) = a\varphi + b \tag{9.6}$$

Almost invariably for a consolidated sandstone, a plot of permeability (k) on a logarithmic scale against porosity (φ) results in a clear trend with a degree of scatter

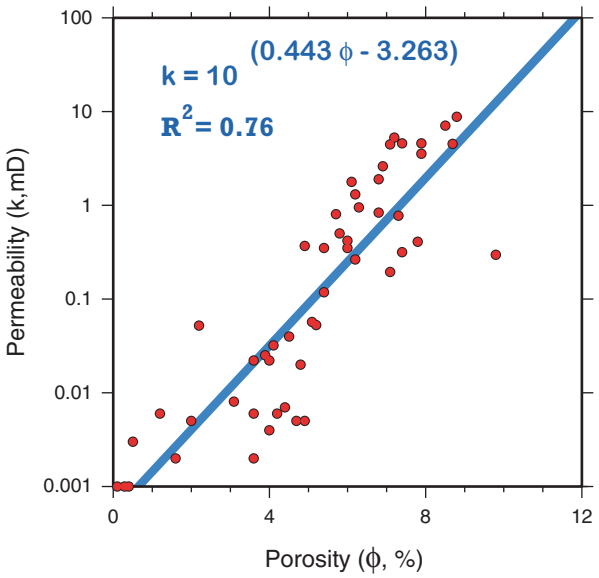

Fig. 9.7 Semilog plot of permeability vs. porosity for the core samples from the Weber Formation, RSU #1 well, Rock Springs Uplift, Wyoming (*red dots*). The corresponding semi-logarithmic regression for permeability k (the line, equation, and coefficient of determination) is shown in blue

associated with the other influences determining the permeability. Fig. 9.7 shows a log (k)-vs.-φ plot for the core samples from the Weber Sandstone. There is a strong linear correlation ($R^2 = 0.76$) between log (k) and φ with a relatively steep trend that is characteristic of "tight gas sands" (Nelson 1994). Clearly, permeability can be predicted from porosity in such an environment.

With insertion of the regression coefficients into Eq. 9.6, the corresponding power-law equation for the Weber Sandstone permeability will be:

$$k = 10^{(0.443\varphi - 3.263)} \tag{9.7}$$

Equation 9.7 was then used to calculate a continuous permeability profile for the Weber Sandstone unit penetrated by the RSU #1 well: porosity estimated from density-log values was used to predict permeability.

The result of modeling is shown in Fig. 9.8. Figure 9.8 also shows other well logs for visual comparison, as well as the core measurements. Although the measured and calculated data sets in Fig. 9.8 do not match perfectly, there is definitely visual correlation between them. For the Weber Sandstone unit, both density-derived and sonic-derived porosities can be used interchangeably for permeability prediction, since strong correlation exists between the density and velocity logs. The permeability profile shown in Fig. 9.8 is characterized by significant variability and a high proportion of low-permeability intervals (with values below 1.0 mD). Overall, the Weber Sandstone in the study area can be classified as a variably permeable, tight formation. The lack of mud cake, as indicated by the caliper log (Fig. 9.8), supports this conclusion.

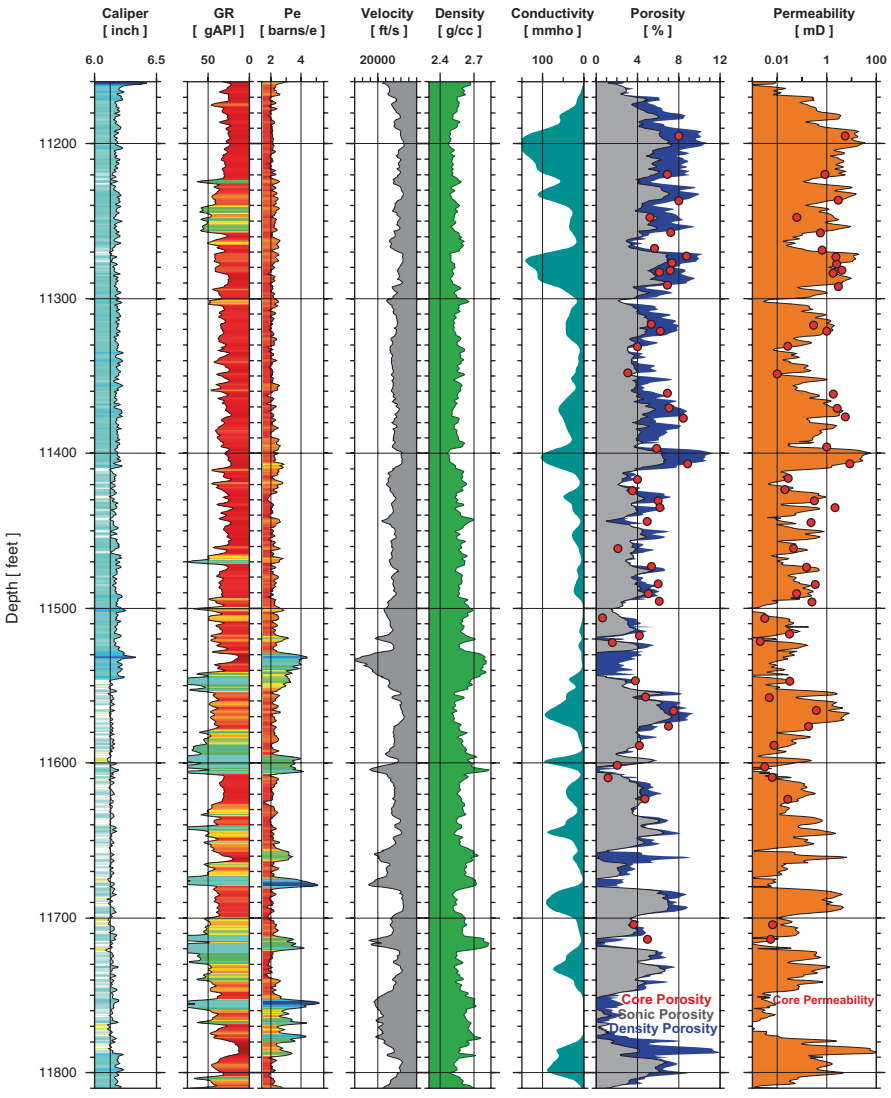

Fig. 9.8 Open-hole logs and core data in the Weber Formation in the RSU #1 well. Tracks from left to right are (1) caliper, (2) gamma-ray, (3) photo electric section, (4) P-wave velocity, (5) density, (6) conductivity, (7) density (*blue*) and sonic (*gray*) porosity with total porosities from core (*red dots*), (8) modeled permeability (*orange*) overlaid with core measurements (*red dots*)

A similar technique of permeability estimation (Eq. 9.7) can be applied to the lateral distribution of porosity values derived from surface seismic (see Chap. 7). The result of permeability modeling for the Weber Sandstone away from the RSU #1 well is shown in Fig. 9.9. Most of the area on the permeability map is blue and yellow, which correspond to permeability values below 1.0 mD (Fig. 9.9b). We note

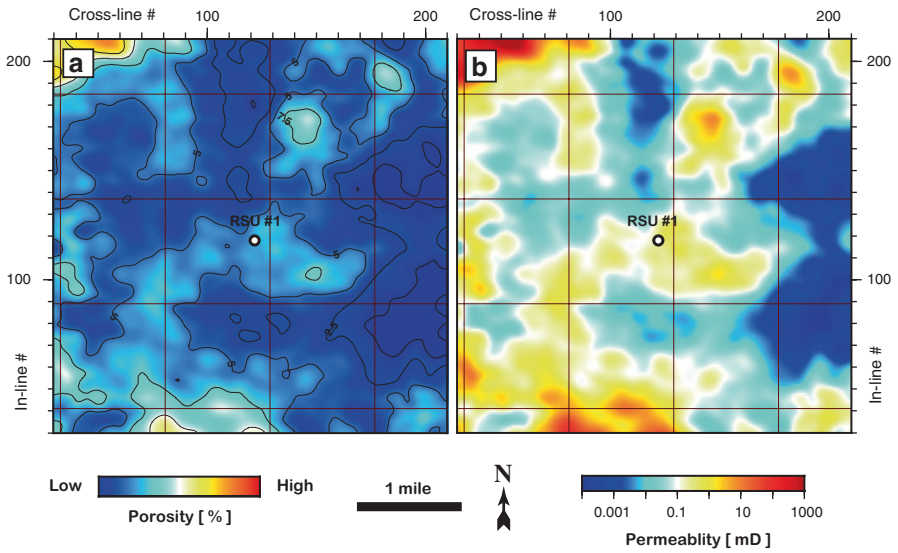

Fig. 9.9 (**a**) Porosity and (**b**) permeability maps on top of the Weber Sandstone stratigraphic unit. For both plots, increases in value correspond to transition from blue to red. Note that peripheral areas are less reliable in attribute estimation due to decreased seismic coverage

that uncertainty in the seismically derived permeability map, due to the absence of control wells, increases away from the RSU #1 well toward the periphery of the seismic study area.

9.2.2 Permeablity Distribution

9.2.2.1 The Weber Sandstone

Plots of petrophysical data vs. depth, e.g, those in Fig. 9.8, can be used to distinguish and separate geologic units. However, many modern flow simulation routines require a general quantitative reservoir descriptor obtained from data samples that are treated as random variables and are not attributed to a specific location. Both the probability and cumulative distribution functions (histograms) are common statistical tools that can be used to derive such a generalized descriptor of a formation. Fig. 9.10 shows histograms of the permeability distribution within the Weber Sandstone, based on estimates per Sect. 9.2.1. We used 1,341 data samples to produce the distributions that correspond to the 670-ft-thick interval, from 11,155 to 11,825 ft in depth.

On a logarithmic scale, the Weber Sandstone is characterized by a multi-peak, slightly right-skewed permeability distribution (Fig. 9.10a). Unlike a normal distribution, the asymmetric one can be described with several averaging estimators:

the arithmetic mean, geometric mean, median, and mode. For a normal distribution all four estimators produce the same number; all four numbers for the Weber Sandstone permeability distribution are different. Our estimators differ greatly, ranging from 0.06 mD for the mode to 1.94 mD for the arithmetic mean. Now, how well do these estimators represent the permeability population?

For the Weber Sandstone permeability, the arithmetic mean is 1.94 mD, which is much greater than the median distribution value, 0.12 mD. According to Jensen et al. (2000), the geometric mean should produce a better estimate for a log-normal distribution. The Weber Sandstone permeability distribution has close to a log-normal shape (only slightly asymmetric); therefore, we might use the geometric mean (0.13 mD) as a statistical permeability estimate for the whole stratigraphic unit. Since the permeability distribution (Fig. 9.9a) is multi-peak, the mode (0.06 mD) is not a useful indicator. The median (0.12 mD) is very close to the geometric mean; hence, we conclude that 0.125 mD (here, the average of the geometric mean and the median) would be the best permeability descriptor for the whole Weber Sandstone section.

The cumulative histogram (Fig. 9.10b) can be used to determine the number of permeability values within a given range that have occurred (interval probabilities). As can be seen in Fig. 9.10b, 50% of the data (samples) have a permeability value ($k_{0.50}$) of about 0.1 mD or less; that is the median value. Only 20% of the data within the depth interval 11,155–11,825 ft (Fig. 9.10) have a permeability value greater than 1.0 mD.

The Dykstra-Parsons coefficient (V_{DP}) is commonly used in the petroleum industry as a measure of permeability variation or reservoir heterogeneity (Jensen et al. 2000). It is defined as

$$V_{DP} = \frac{k_{0.50} - k_{0.16}}{k_{0.50}}, \tag{9.8}$$

where $k_{0.50}$ is the median permeability and $k_{0.16}$ is the permeability one standard deviation below the median on a log-probability plot. V_{DP} ranges between zero (0.00) for absolutely homogeneous reservoirs and one (1.00) for "infinitely" heterogeneous reservoirs. With a V_{DP} of 0.91, the Weber Sandstone can be considered a highly heterogeneous reservoir rock.

9.2.2.2 The Madison Limestone Reservoir

The corresponding statistical permeability estimates for the middle Madison unit are listed in Fig. 9.11. This carbonate reservoir is characterized by a wide, multi-peak, left-skewed permeability distribution. The asymmetry of the distribution is much more pronounced than that of the Weber Sandstone unit. The difference between the mode and the geometric mean of the Madison permeability distribution exceeds 20 mD (Fig. 9.11a). We chose the median permeability value of *3.25 mD* as the most appropriate average permeability estimate. However, even the lowest

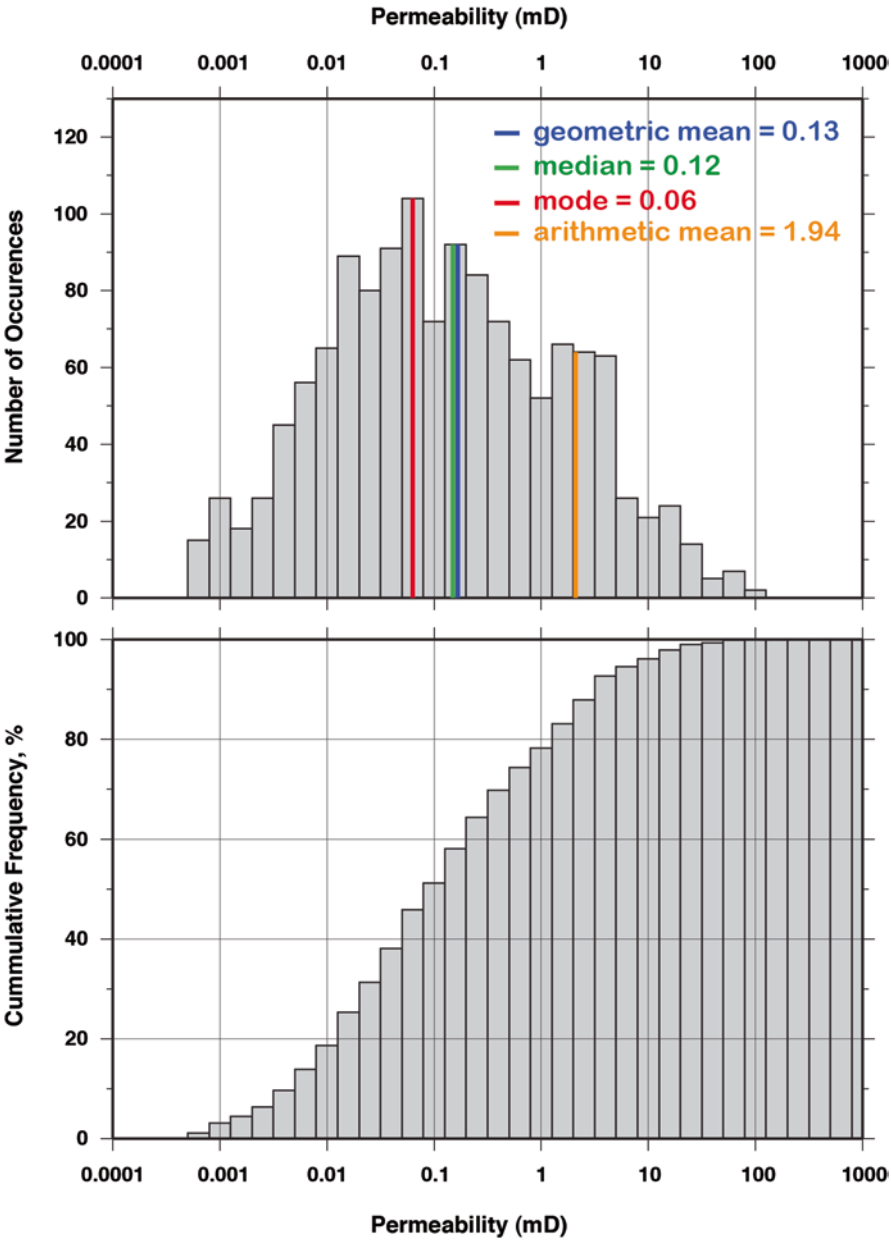

Fig. 9.10 Permeability distribution within the Weber Sandstone unit (11,155–11,825 ft depth interval; 1,341 data samples). Ordinary histogram (*top*); cumulative histogram (*bottom*)

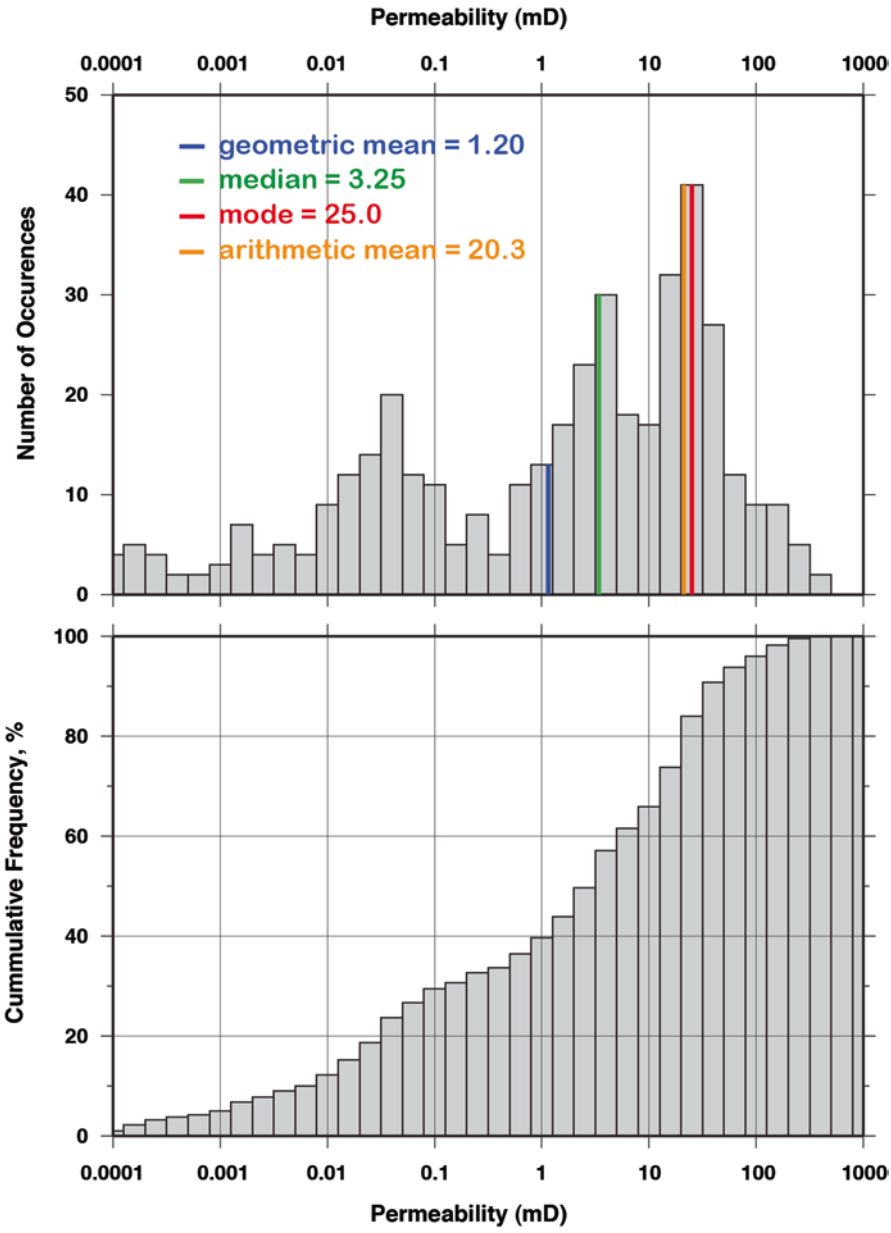

Fig. 9.11 Permeability distribution within the middle Madison unit (12,340–12,540 ft depth interval; 401 data samples). Ordinary histogram (*top*); cumulative histogram (*bottom*)

descriptor for the middle Madison reservoir—the geometric mean (1.2 mD)—is an order of magnitude higher than the Weber Sandstone permeability estimate. The cumulative histogram indicates that 60 % of the data within the depth interval 12,340–12,540 ft ( ) have permeability values greater than 1.0 mD. On the basis of permeability statistics, we conclude that the middle Madison unit has much better reservoir properties than does the Weber Sandstone. The estimated Dykstra-Parsons heterogeneity index (V_{DP}) for the middle Madison depth interval (12,340–12,540 ft) is 0.99, which characterizes this reservoir as extremely heterogeneous.

References

Amaefule JO, Altunbay M, Taib D, Kersey DG, Keelan DK (1993) Enhanced reservoir description: using core and log data to identify hydraulic (flow) units and predict permeability in uncored intervals/wells. Paper SPE 26436, presented at the SPE 68th annual technical conference and exhibition, Houston. 3–6 October, Texas 1993

Anselmetti FS, Eberli GP (1999) The velocity-deviation log: a tool to predict pore type and permeability trends in carbonate drill holes from sonic and porosity or density logs. AAPG Bull 83(3):450–466

Archie GE (1950) Introduction to petrophysics of reservoir rocks. AAPG Bull 34(5):943–961

Bird RB, Steware WE, Lightfoot EN (1960) Transport phenomena**.** Wiley, New York

Carmen PC (1937) Fluid flow through granular beds. Inst Chem Eng Trans 15:150–166

Doveton JH (1994) Geologic log interpretation—reading the rocks from wireline logs. Soc Econ Paleontol Miner Short Course 29

Ehrenberg SN, Eberli GP, Keramati M, Moallemi SA (2006) Porosity-permeability relationships in interlayered limestone-dolostone reservoirs. AAPG Bull 90(1):91–114

Gunter GW, Finneran JM, Hartmann DJ, Miller JD (1997) Early determination of reservoir flow units using an integrated petrophysical method. Paper SPE 38679, presented at the 1997 SPE annual technical conference and exhibition, San Antonio, Texas, 5–8 October

Guo G, Diaz MA, Paz F, Smalley J, Waninger EA (2007) Rock typing as an effective tool for permeability and water-saturation modeling: a case study in a clastic reservoir in the Oriente Basin. SPE Reserv Eval Eng 10(6):730–739

Hartmann DJ, Farina J (2004) Integrated reservoir analysis: Predicting reservoir performance through collaboration. Occidental Oil & Gas Corporation, Houston, Texas, course workbook

Jennings JW Jr, Lucia FJ (2001) Predicting permeability from well logs in carbonates with a link to geology for interwell permeability mapping. Paper SPE 71336, presented at the SPE annual technical conference and exhibition, New Orleans, 30 September–3 October. DOI: 10.2118/71336-MS

Jensen JL, Lake LW, Corbett PWM, Goggin DJ (2000) Statistics for petroleum engineers and geoscientists, 2nd edn. Handbook of petroleum exploration and production, 2. Elsevier, Amsterdam

Kolodzie S Jr (1980) Analysis of pore throat size and use of the Waxman-Smits equation to determine OOIP in Spindle Field, Colorado. Paper SPE 9382

Lucia FJ (1999) Carbonate reservoir characterization. Springer-Verlag, New York

Mavko G, Mukerji T (1995) Seismic pore space compressibility and Gassmann's relation. Geophysics 60:1743–1749

Nelson PH (1994) Permeability-porosity data sets for sandstones. Lead. Edge (23):1143–1144

Nelson PH (2004) Permeability-porosity relationships in sedimentary rocks. Log Anal.(May–June):38–62

Porras JC, Campos O (2006) Rock typing: a key for petrophysical characterization and definition of flow units, Santa Barbara field, eastern Venezuela Basin. Paper SPE 69458, presented at the 2001 SPE Latin American and Caribbean petroleum engineering conference, Buenos Aires, 25–28 March 2001. DOI: 10.2118/69458-MS

Prasad M (2003) Velocity-permeability relations within hydraulic units. Geophysics 68(1):108–117
Rider MH, Kennedy M (2011) The geologic interpretation of well logs, 3rd edn. Rider-French Consulting Ltd., Scotland
Schlumberger (1974) Log interpretation—applications, vol. 2. Schlumberger Limited, New York
Weger RJ, Eberli GP, Baechle GT, Massaferro JL, Yue-Feng S (2009) Quantification of pore structure and its effect on sonic velocity and permeability in carbonates. AAPG Bull 93(10):1297–1317
Wyllie MR, Gregory AR, Gardner GHF (1956) Elastic wave velocities in heterogeneous and porous media. Geophysics 21(1):41–70
Xu C, Russell D, Gournay J, Richter P (2006) Porosity partitioning and permeability quantification in vuggy carbonates using wireline logs, Permian Basin, West Texas. Petrophysics 47(1):13–22;